ACS Photonics

Article

pubs.acs.org/journal/apchd5

On-Demand Surface- and Tip-Enhanced Raman Spectroscopy Using Dielectrophoretic Trapping and Nanopore Sensing

Kevin J. Freedman,[†,⊥] Colin R. Crick,[†,⊥] Pablo Albella,[‡] Avijit Barik,[§,∥] Aleksandar P. Ivanov,[†] Stefan A. Maier,[‡] Sang-Hyun Oh,[§,∥] and Joshua B. Edel*[,†]

[†]Department of Chemistry and [‡]EXSS Group, Physics Department, Imperial College London, South Kensington, SW7 2AZ, London, United Kingdom

[§]Department of Electrical and Computer Engineering and [∥]Department of Biomedical Engineering, University of Minnesota, Minneapolis, Minnesota 55455, United States

Supporting Information

ABSTRACT: Surface-enhanced Raman spectroscopy (SERS) and tip-enhanced Raman spectroscopy (TERS) have shown great promise in the detection and analysis of trace analytes throughout numerous fields of study. Both SERS and TERS utilize nanoscale plasmonic surface features to increase the intensity of observed Raman signals by many orders of magnitude (>10^8). One of the major factors limiting the wider and more routine implementation of the enhanced Raman phenomena is in the difficulty of forming consistent and reliable plasmonic substrates with well-defined "hot-spots". We address this limitation by designing a platform that can be used for both SERS and TERS. The presented technique allows for rapid, controlled, "on-demand", and reversible formation of a SERS substrate using dielectrophoresis at the end of a nanoscale pipet. This drives gold nanoparticles in solution to concentrate and self-assemble at the tip of the pipet, where analytes can be detected effectively using SERS. An additional benefit of the platform is that the nanopipet containing a nanopore can be used for detection of individual nanoparticles facilitated by the added enhancement originating from the nanopipet tip enhanced signal. Complementing the experimental results are simulations highlighting the mechanism for SERS substrate formation and TERS detection.

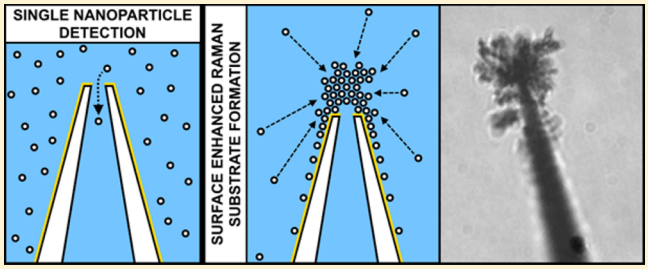

KEYWORDS: *surface-enhanced Raman spectroscopy, SERS, TERS, DEP, nanopipet, gold nanoparticles, translocation*

The vibrational modes of a chemical bond provide extremely precise information about a molecule. Achieving higher signal strength from fewer molecules has been the driving force behind developing Raman amplifiers such as nanoscale metallic features (i.e., surface-enhanced Raman spectroscopy, SERS) or ultrasharp tips (i.e., tip-enhanced Raman spectroscopy, TERS).[1−5] In both cases, signal amplification is caused by the electromagnetic (EM) fields generated and focused to a localized region.[6] The scientific literature details a multitude of methods in forming SERS substrates; however agglomerations of plasmonic nanoparticles (gold/silver) have been proved to be among the most successful examples.[5,7,8] The majority of these lack control over deposition; particles are distributed randomly over the underlying material. Inefficient assembly of nanostructures stems from the fact that nanosensors (as well as all sensors whose "detection zone" is on the order of a nanometer) are diffusion-limited.[9] In light of these problems, there is a need to develop methods to allow controllable, reversible, and on-demand assembly of SERS substrates. Raman spectroscopy is a longstanding method for probing specific chemical properties of a molecule. SERS spectra can be used to identify functional groups as well as their structural dynamics in a multiplexed and label-free manner.[10] Although nanopores, atomic force microscopy, and optical tweezers are among a set of methods which can obtain both single-molecule (SM)[11−15] and submolecular information,[16,17] SERS provides very unique spectra for a target molecule. The vibrational modes of a molecular bond therefore provide a fingerprint for the detection of trace analytes.

Previous work has shown the ability to self-assemble nanoparticles within an aqueous environment, creating close-packed nanoparticle arrays that greatly enhanced SERS detection capabilities.[18] DNA origami-based assembly of nanoparticles has also been shown to be successful by other groups.[19,20] Another powerful technique exploited for nanoparticle aggregate assembly is dielectrophoresis (DEP), which can act to readily concentrate solution-based moieties (molecules/particle) under the action of an ac voltage. DEP allows for charged and neutral species to be manipulated over micrometer length scales,[21] making concentrating particles particularly efficient.[22] Making use of the polarizability of a

Received: February 19, 2016
Published: May 10, 2016

DOI: 10.1021/acsphotonics.6b00119
ACS Photonics 2016, 3, 1036−1044

particle, DEP attracts (positive DEP, or pDEP) or repels (negative DEP, or nDEP) objects in a nonuniform electric field toward or away from the point of maximum field intensity, respectively.

Nanopore technology is particularly attractive for plasmonic studies due to the confinement of single-molecule events to a localized optical plane/position.[23−25] Nanopipets, in particular, are a class of biosensors possessing a nanopore at the head of a sharp (nanoscale) tip that have been utilized in SERS experiments,[26,27] among other applications.[21,28−32] The advantages provided by SERS can be extended by exploiting the sharp tips of these nanopipet devices, in a technique called TERS. TERS, in principle, helps eliminate the need to construct nanoscale features with high surface roughness from metallic building blocks. Using sharp nanoscale spikes constructed from plasmonically active materials, TERS can be achieved by facilitating tip-localized SERS. Simulations of the EM field for different tip sizes (tip radii of 5−75 nm) revealed that tips with a radius of <75 nm can be used for TERS, opening the door for using nanopipets.[33] These types of devices have been shown to provide enhancement factors (EF) in the range of 10^6−10^7 and even higher.[34] This level of signal amplification approaches the SM level; however, it is well recognized that methods that provide greater control of the size, shape, and formation of the TERS tips are required.[35,36]

The majority of literature examples, reporting SERS/TERS using nanopipets, use nanoparticles deposited randomly on the outer surface of the pipet via electrostatic binding. Using such a device for in situ measurements of intracellular environments is possible and was demonstrated by Vitol et al.[26] The authors of this work accurately state that the advantage of using nanopipets for SERS applications is that nanopipets allow for the simultaneous injection of drugs and/or toxins while measuring the cells' response in real time. With the aim of making SERS nanopipets specific to a known target protein, one particular variation of this technology would be a SERs immunoassay. This demonstrates that specificity can be imparted to SERS sensing.[27] Strategies to enhance SERS signals have also been widely reported on and demonstrated using surface binding in a microfluidic device,[37] electrophoresis on a microfabricated surface,[38] surface-tension-driven concentration in metallic nanohole arrays,[39] and dielectrophoresis on microelectrodes[40] or sharp pyramidal tips.[41] Nanopipets, however, offer several benefits over the above 2D SERS substrates including (1) intrinsic tip enhancements,[42] (2) well-defined 3D location of a SERS hot-spot,[41,43] (3) mobility of the SERS hot-spot,[41] (4) molecular delivery from inside the nanopipet[28] (e.g., single-molecule delivery onto a SERS substrate), and (4) single-molecule measurements of intracellular components[44] (via translocation and electrical signal read-out).

In this report, two major advances in surface-bound analyte examination are demonstrated. The first stems from DEP-active Au-coated nanopipets acting on a suspension of gold nanoparticles, which are capable of providing on-demand SERS substrate formation. More specifically, it allowed for the control of the size, shape, and rate of formation of gold nanoparticle (AuNP) aggregates at a well-defined hot-spot for SERS (i.e., the tip of the nanopipet). Second, TERS was observed upon passing individual gold nanoparticles through the nanopore atop the nanopipet. Each translocation event was identified as a peak in Raman intensity. Each of these phenomena was supported by simulations of the DEP and electromagnetic field enhancement, respectively. Despite finding that nanopipets are ideally suited to act as a DEP electrode, nanopipets have yet to be explored in this context.

RESULTS AND DISCUSSION

The experimental approach used in this study incorporates ionic and electrically conducting nanopipets (Figure 1a) with aqueous SERS substrates (AuNP) for (1) single-particle translocations detected using TERS and electrical measurements (Figure 1b) and (2) the on-demand AuNP assembly for SERS sensing (Figure 1c). AuNP assembly was accomplished using DEP and served to increase the SERS signal of a bound analyte through creating a concentrated plasmonic substrate. Both parts of this study were performed using quartz capillaries pulled to a diameter of approximately 70 nm (Figure 1d). Pipets were coated with 5 nm of gold via sputtering after the pulling procedure to make them electrically conductive. The position of the tip was controlled using an XYZ micro-

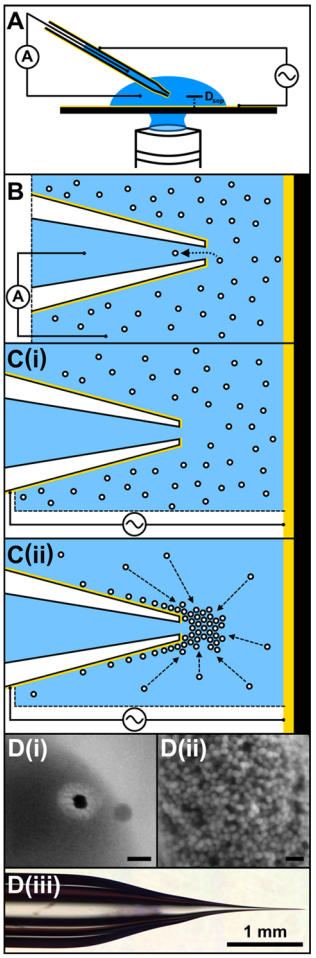

Figure 1. (a) Schematic representation of the DEP-enhanced SERS nanopipet system. (b) Schematic of single AuNP translocation, detected using TERS, using an electrically biased nanopipet. (c) Schematic of the nanopipet at the start of experiments (c(i)) and following DEP-induced aggregation of AuNP at the tip of the nanopipet (c(ii)). (d) SEM and optical microscopy (i) SEM image of a nanopore (Ø = 70 nm) on the gold-coated nanopipet, (ii) SEM image of aggregated AuNPs at the nanopipet tip, and (iii) used for translocation and DEP experiments. Scale bars (unless otherwise stated) show 100 nm.

DOI: 10.1021/acsphotonics.6b00119
ACS Photonics 2016, 3, 1036−1044

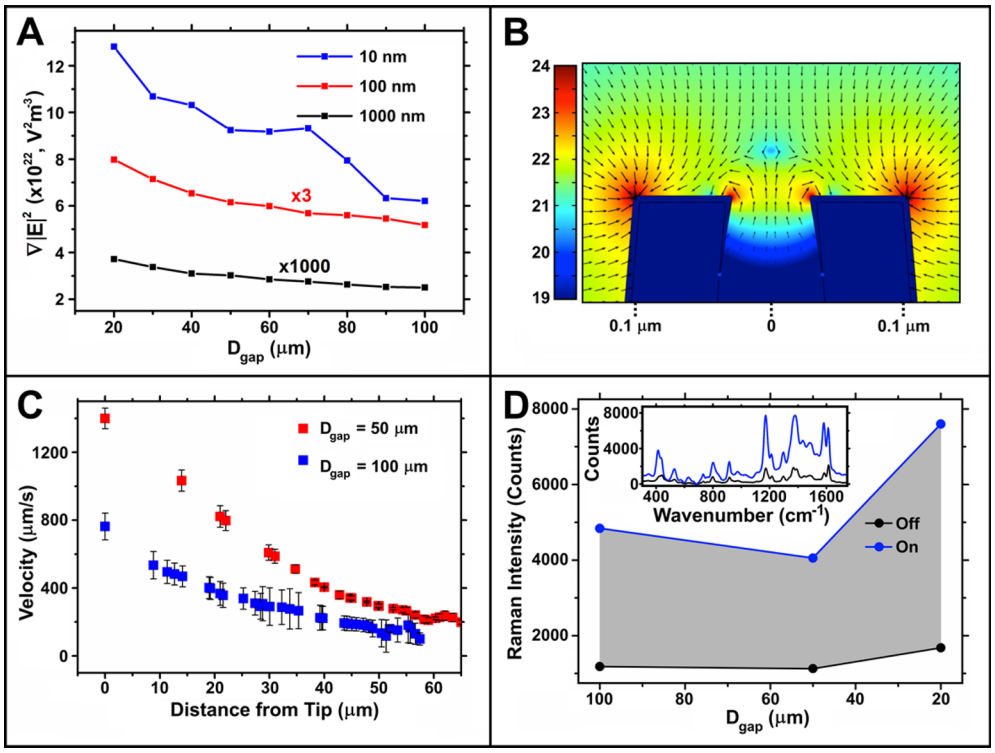

Figure 2. Influence of device geometry on AuNP trapping and SERS enhancement. (a) Gradient of electric field squared, $\nabla|E|^2$, at 10, 100, and 1000 nm from the tip of the nanopipet as a function of electrode gap distance, D_{gap}. The data collected at 100 and 1000 nm from the tip were multiplied by 3 and 1000, respectively, to show the trends of each line on the same graph. (b) Logarithmic colormap image of $\nabla|E|^2$ in units of V^2 m^{-3}. The logarithmically scaled arrows depict the direction of the DEP force, which is proportional to the $\nabla|E|^2$. (c) Particle tracking of fluorescent AuNPs at two electrode gap distances. Velocity profiles are plotted as a function of the distance between the AuNP and the nanopipet tip. (d) SERS measurements of three different nanopipets during periods of no DEP trapping ("Off") and periods of DEP trapping ("On").

manipulator (PT3/M-Z7, Thorlabs), and the distance from the ground electrode (a glass slide coated with 5 nm of gold) was determined using optical microscopy. DEP trapping was initiated through the application of an ac voltage bias between the two Au electrodes (Figure 1c). Once the tip was submerged in KCl, a current−voltage (I−V) curve was generated to confirm that the nanopore is intact and conducting (Figure S1, Supporting Information). The pipets used in this study had a resistance of 117 ± 12 MΩ (measured in 10 mM KCl, 10 mM Tris/EDTA, pH 8, between −600 and 600 mV; average of 10 nanopipets) and a pore diameter of 70 nm as measured by SEM (Figure 1d). Once the electrical characteristics of the nanopipet were quantified, the nanopipet tip was submerged in a solution of gold nanoparticles (see Methods[45] on AuNP synthesis, diameter ∼43 nm) functionalized with malachite green isothiocyanate (MGITC). Control experiments using 4-mercaptobenzoic acid, as well as spectra for functionalized AuNPs dried on a glass substrate, can be found in the Supporting Information (Figures S2, S3). UV−vis was used to ensure that the MGITC did not cause the AuNPs to aggregate prior to DEP trapping. When MGITC was added such that there were >2000 MGITC molecules per AuNP, the particles would visually fall out of solution. However, a 10× dilution of MGITC (∼297 MGITC molecules per particle) retained stability for several hours to days (Figure S1, Supporting Information).[45]

Surface-Enhanced Raman Spectroscopy Using DEP. DEP forces are capable of trapping particles or molecules at the tip while an alternating electric field is applied to the pipet. Due to the weakening of the electric field when propagating through space, the distance between the tip of the nanopipet and the ground electrode, D_{gap}, is a critical parameter that determines the force on particles and therefore the rate of accumulation. The magnitude of the force on the particle scales with the electric field gradient and was used to understand the dependence of D_{gap} on the attractive force on the particles. DEP forces were first investigated by simulating the electric field gradient, $\nabla|E|^2$, along the z axis extending out from the nanopipet tip toward the ground electrode. The dependence of $\nabla|E|^2$ is shown for changing electrode gap distances (D_{gap} = 20−100 μm) at positions 10, 100, and 1000 nm from the tip (Figure 2a). At all the positions tested, the smaller D_{gap} conditions exhibited larger electric field gradients, suggesting particles would (a) accelerate toward the tip faster and (b) overcome diffusion further away from the nanopipet tip (i.e., form a larger capture radius). Function fitting shows a logarithmically decreasing trend in the force as the electrode gap distance increases, which matches our expectations based on previous literature.[46,47] From the vector map of the electric field gradient (Figure 2b), it is also apparent that the point of highest force, and the location of DEP trapping, is at the nanopipet tip itself. Once diffusion is overcome, DEP forces are capable of trapping particles or molecules at the tip, for as long as an alternating electric field is applied to the pipet.

Simulated data were supported experimentally using two approaches: particle tracking and SERS measurements. Particle tracking was achieved using fluorescently labeled 40 nm AuNPs (Nanopartz Inc.) and tracking the centroid position of the particles in relation to the distance from the tip (averaged over 20 particle trajectories; see Supporting Information for full

DOI: 10.1021/acsphotonics.6b00119
ACS Photonics 2016, 3, 1036−1044

details). For D_{gap} values of 50 and 100 μm, the velocity of the AuNPs increases linearly as the particles approach the tip of the nanopipet (Figure 2c). This supports the simulation data, which indicated that the nanopipet tip has the highest electric field gradient and therefore acts as the point of local attraction. More importantly, as D_{gap} was reduced, particles reached higher velocities, indicating that the DEP force is stronger when the nanopipet is close to the ground electrode. Since the DEP force scales linearly with the electric field gradient emanating from the tip, DEP forces can be maximized by reducing D_{gap}.

The distance dependence of nanoparticle agglomeration was confirmed using SERS measurements of MGITC-functionalized AuNPs using a 632.8 nm laser positioned directly on the tip of the nanopipet. Once a baseline measurement was obtained, DEP trapping was achieved by applying an ac voltage (10 V, 1 MHz) to the gold electrodes. For each of the three D_{gap} conditions tested, a fresh nanopipet was used. All three baseline measurements (Figure 2d; "off" conditions) consistently yielded low photon counts (i.e., low SERS signal) and represented the variability typically observed between different nanopipets. After DEP trapping, the EF was largest for a D_{gap} of 20 μm (minimal change was observed between 50 and 100 μm). For all further studies, a D_{gap} of 20 μm was used unless otherwise stated, owing to the higher electric field gradients at lower electrode gaps.

Upon characterization of the gap distance, DEP parameters (ac frequency and voltage) should be selected based on the complex dielectric constants of the nanoparticle and the medium in which the particles are suspended. This is common procedure for most polarizable nanoparticles such as those composed of polystyrene. Since AuNPs are always more polarizable than low-conductivity solutions, we expect a positive DEP response across the operating frequency range.[48] Upon applying an ac bias to the nanopipet, an aggregate of AuNPs formed locally around the nanopipet tip (Figure 3a). Diffusion took over after DEP was turned off, and this led to a gradual loss of AuNPs from the nanopipet tip. Scanning electron micrographs (Figure 3b) show a small cluster of AuNPs that remain at the tip of the nanopipet acting as a SERS hot-spot in DEP experiments. Throughout DEP trapping experiments and subsequent SEM imaging, it was observed that AuNP coverage (i.e., surface area covered with particles) and density (i.e., the number of particles in one area) increased with DEP trapping time (diffusion-induced collisions alone did not result in AuNP adsorption). Particles adsorbed to the surface only when DEP forces were applied, originating first at the tip and traveling up the shaft of the pipet tip. For prolonged DEP trapping in which the SERS signal saturates (e.g., Figure 3c), both the coverage and density increased significantly (Supporting Information Figure S4). In Figure 3b, the AuNP cluster extends 1 μm from the tip for ~1 min of DEP trapping and ~50 μm from the tip for 10 min of DEP trapping. It is important to note that DEP-enhanced SERS does not require large AuNP clusters, and DEP trapping times should be optimized based on AuNP concentration.

Previous work in the literature has utilized electrostatic binding of AuNPs on the surface of nanopipets, therefore, it is important to compare the results between both electrostatic[26,27] and DEP-assisted AuNP coatings. Electrostatic methods rely on random adsorption to the entire surface of the nanopipet. Also, coverage increases as a function of AuNP exposure time (5 h of incubation with AuNPs is needed to acquire a dense AuNP coating on the nanopipet).[26] The

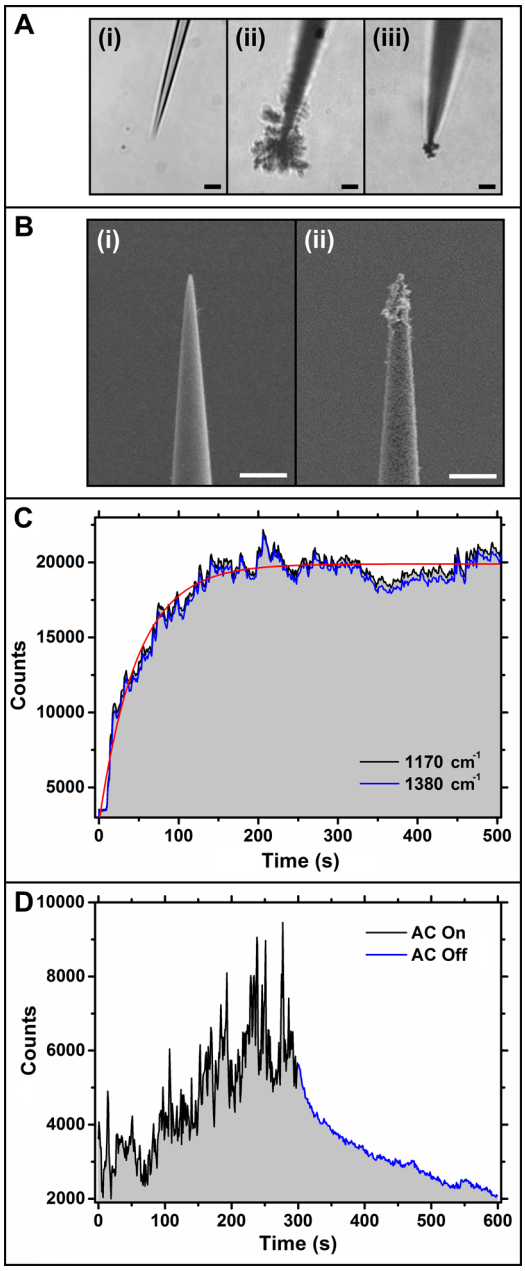

Figure 3. (a) Light microscopy images of the nanopipet before (i), during (ii), and after (iii) DEP-induced AuNP aggregation. Scale bars show 20 μm. (b) SEM images of a nanopipet before (i) and after (ii) a single DEP trapping experiment (~5 min of trapping) with undiluted Au nanoparticles. Scale bars show 1 μm. (c) Time-tracking of the 1170 cm^{-1} peak over time (DEP was turned on at $t = 0$). (d) Photon counts observed over time with DEP turned off at $t = 300$ s, leading to a decay in SERS enhancement.

coverage obtained in this study is significantly higher, localized to the tip, and occurs within 2−3 min of DEP trapping or less depending on the desired level of coverage and particle density.

On-demand DEP-enhanced SERS yielded an EF of at least 16 000 compared to control measurements without using DEP (Figure S2, Supporting Information; D_{gap} = 20 μm, 10 V, 1 MHz). Tracking of the 1170 cm^{-1} Raman peak (corresponding to the bending of the C−H bond) provided measure of the kinetic growth of AuNP aggregation locally around the nanopipet tip (Figure 3c).[10] The peak increases exponentially upon turning on DEP and levels off after 150 s, staying

DOI: 10.1021/acsphotonics.6b00119
ACS Photonics 2016, 3, 1036−1044

approximately at the same level for the remainder of the experiment (5.8 min). The observation that SERS enhancement reaches a maximum is likely due to the fact that the laser spot has a fixed size. As a result, the volume of AuNPs that scatter photons is also bounded by the laser spot. Equivalent data (as shown in Figure 3) were also obtained using silver NPs (see the Supporting Information).

Visualization of the SERS decay after DEP trapping was accomplished by tracking a SERS peak for one DEP on/off cycle (total of 10 min). An exponential drop in the peak intensity was observed until the peak reached baseline values (Figure 3d). Although it is unclear whether every AuNP was removed from the pipet, clogging of the pore is always a concern when dealing with nanopores. Preventing AuNPs from blocking the nanopipet tip can be feasibly accomplished by reducing AuNP concentrations or applying a high trans-pore voltage (as used later for translocation experiments). Pulsing DEP between SERS measurements and translocation experiments in repetition is the ideal system wherein AuNPs can be probed for an analyte molecule and electrical measurements of single particles can be obtained.

In order to gain a better understanding of the SERS substrate formation kinetics, DEP pulsing was lowered from a pulse duration of 300 s (the longest pulse duration) down to 5 s (the shortest pulse duration). The inability for the signal to reach the baseline at the end of the "DEP off" cycle led to the hypothesis that DEP concentrates AuNPs faster than they can diffuse away. The result is that the SERS signal never reaches the pre-DEP level and starts the next cycle at an already enhanced level (Figures 4a,b). To test this, a model of the diffusion process was formulated (details supplied in the Supporting Information). The model assumed independent steady-state conditions for both the "DEP on" phase and the "DEP off" phase. This is accompanied by a fixed capture rate of AuNPs when DEP was on and steady-state diffusion when DEP was off. The number of AuNPs inside a fixed volume (using an approximation of the laser spot size) was calculated, normalized, and plotted over time (Figure 4bii). Since there is a fixed volume in which particles can fit inside, a fixed maximum level was achieved for both the SERS signal and the normalized particle concentration. On the basis of the laser spot diameter of ~2 μm and the spherical growth of the AuNP aggregate, the maximum number of particles in the laser spot corresponds to approximately 70 000 AuNPs (assuming a maximal packing efficiency of ~0.74). It should be noted however that laser transmission through such a large AuNP aggregate would be low, resulting in photons being collected only from the outermost shell that faces the laser. In the model, diffusion initially led only to a 38% reduction of AuNPs inside the approximated laser spot, leading to AuNP assembly (i.e., buildup) across cycles (assuming 5 s of DEP and 5 s of no DEP). As the AuNP concentration grew over time, the concentration gradient also became larger until eventually, and irrespective of model parameters, the flux of particles out of the laser spot equaled the rate of influx due to DEP. The number of cycles required to fill the laser spot, however, did depend on the model parameters (i.e., cycle time, DEP capture rate, etc.), with our best approximations leading to equilibrium after 5 cycles (D = 10 μm^2/s, DEP capture rate = 220 particles/s, cycle duration = 10 s; details provided in the Supporting Information). These experiments demonstrated that DEP-enhanced nanopipets are a versatile technique to capture and assemble AuNPs for SERS applications on short (s) time scales.

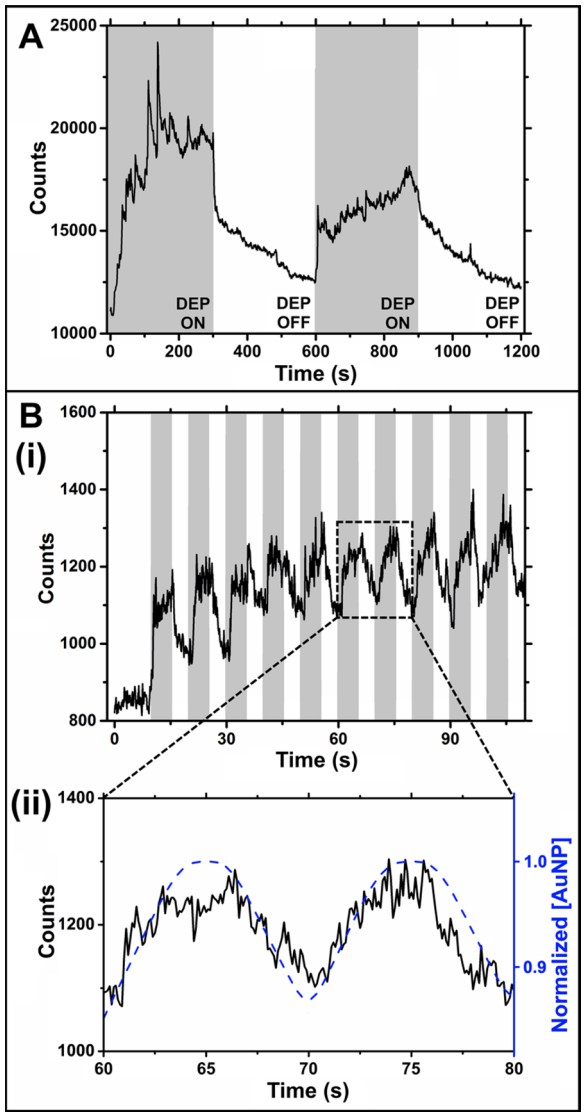

Figure 4. Photon counts observed over time with DEP turned on/off with varying cycle parameters. (a) Time-tracking of the 1170 cm^{-1} peak over the course of a 20 min recording using a pulse duration of 300 s (DEP was turned on at t = 0 in each experiment). SERS enhancement decays during the "off" cycle. (b) On/off DEP pulsing with a DEP pulse duration of 5 s (i). The 1170 cm^{-1} peak was tracked using a time resolution of 100 ms. (ii) Experimental data shown in (i) compared to diffusion model results based on the diffusion of nanoparticles away from a point source (dotted line). Diffusion model parameters: D = 10 μm^2/s, DEP capture rate = 220 particles/s, cycle duration = 10 s.

Translocating Single Particles. The enhancement of Raman signals is governed by the molecule's proximity to a plasmonic feature. In the previous section, the plasmonic SERS substrate was formed from single nanoparticles aggregating via DEP forces. This section however focuses on the TERS enhancements associated with a single particle translocating through the tip of a Au-coated nanopipet/nanopore. Furthermore, during translocation, interactions between the analyte and the nanopore have been shown to play a significant role in the passage time or dwell time of the analyte.[49] To demonstrate how analyte−pore interactions can lead to plasmonic coupling in the nanopipet device geometry, simulations were conducted where the pipet is angled toward

DOI: 10.1021/acsphotonics.6b00119
ACS Photonics 2016, 3, 1036−1044

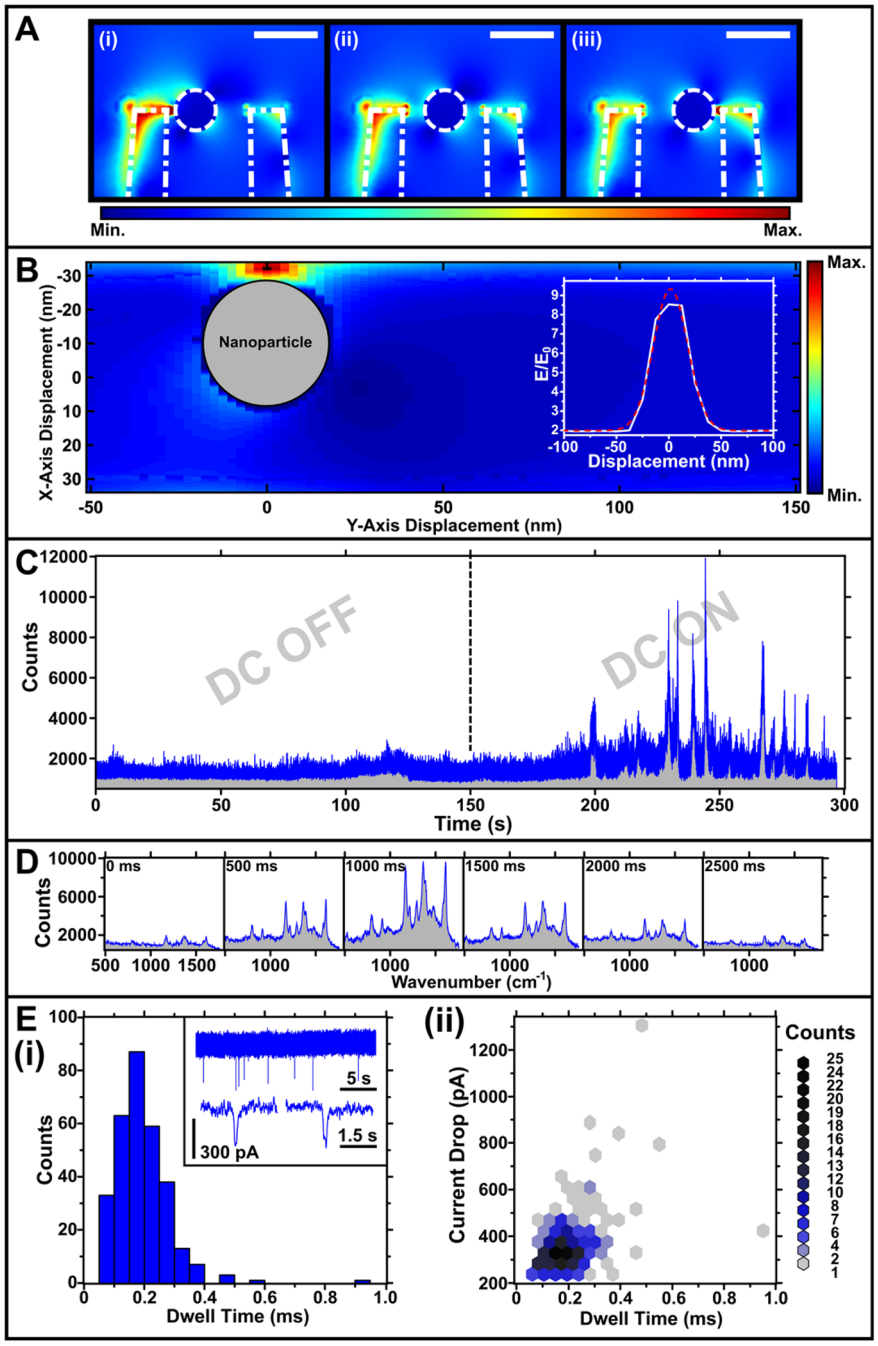

Figure 5. (a) Electric field enhancement (E/E_o) tracked during a AuNP translocation event. Scale bar = 50 nm. (b) COMSOL simulations of the plasmonic coupling during a translocation event. Inset: Normalized electric field versus nanoparticle displacement. (c) Total photon counts showing the translocation of Au nanoparticles only during the application of electrophoretic force. Translocation events occurred only when a negative 200 mV was applied to the electrode inside the nanopipet. (d) SERS spectra at various time points of a Au nanoparticle functionalized with MGITC translocating through the nanopipet tip. (e) Histogram (i) of the dwell time parameter and (ii) a scatter plot of the ionic current drop versus dwell time for MGITC-functionalized Au nanoparticles of the same concentration as the SERS experiments. Inset: Representative current signatures for the translocation of a single AuNP.

a flat gold electrode and irradiated with a polarized laser (see Supporting Information for more details). Plasmonic enhancement was measured as an increase in the electromagnetic field intensity surrounding the AuNP. Compared to AuNPs alone, the EM field intensity surrounding the AuNP increases approximately 8.5 times when translocating through a gold-coated nanopipet (Figures 5a,b). During translocations, EM fields between the gold layer on the pipet and the AuNP increase above baseline values (those observed when a AuNP was irradiated separately; see Supporting Information, Figure S6), indicating a coupling effect between the two gold structures (Figure 5c). One advantage of nanopore sensing is that the detection of a molecule is localized to a fixed, and typically small, volume of space. TERS coupling between the tip and the AuNP is also extremely localized in space, suggesting that both Raman measurements and ionic current measurements are capable of measuring the same translocation event simultaneously.

DOI: 10.1021/acsphotonics.6b00119
ACS Photonics 2016, 3, 1036−1044

Single-particle translocation experiments were performed by placing MGITC-functionalized AuNPs inside the barrel of the nanopipet and applying a negative voltage (−200 mV) to the electrode inside the pipet. The AuNP translocated through the pore in the direction of the electrophoretic force on the particles. Single-particle translocation events were observed, both in the Raman signal and in the ionic current electrical signal (Figure 5). No events were observed prior to applying a voltage bias (Figure 5c). Indicating that limited laser transmission into the barrel of the pipet, or AuNPs, is sterically hindered from entering the region closest to the tip, as observed with DNA in previous work.[28] This represents a significant improvement over membrane-fabricated metallic nanopores since there is no longer a need to use picomolar concentrations of AuNP to prevent random collisions with the nanopore entrance causing unwanted spikes in the Raman signal.[45]

AuNP translocation events occurred roughly at the same frequency for Raman experiments (7.4 events/min) as for ionic current measurements (8.4 events/min). The similarity in event rate suggests that the dc voltage (200 mV in both experiments) applied across the nanopore pulls AuNPs toward the pore at a similar rate. Translocation events taking place while the laser spot is focused on the nanopipet tip, however, caused longer SERS enhancements (>500 ms), typically too long for electrophoretic events (Figure 5d). The laser-illuminated nanopipet therefore showed similar event rates but slower translocation kinetics compared to traditional nanopore experiments. Although unconfirmed, it is possible that the laser spot produces an optical trapping force that could be slowing down particles. Since the laser powers used in this study (single mW range) are much lower than those typically used in optical tweezer setups, we believe that the complete trapping of particles (i.e., halted movement) in the midst of a superimposed dc electric field from inside the nanopore is unlikely. However, the optical gradients are likely to deflect or alter the course of a translocating AuNP, leading to slower event durations and greater interactions with the nanopipet surface. This interpretation assumes that the optical force does not affect AuNP aggregation and is consistent with the lack of nanopore clogging events in both the Raman and ionic current measurements. This effect, examined using DNA, was discussed in detail most recently by Belkin et al.[50]

Translocation events without the laser spot on the tip of the nanopipet were shorter in duration than those with the laser turned on, as discussed previously. The average dwell time and current drop for AuNPs functionalized with MGITC was 209 ± 380 μs and 344 ± 78 pA, respectively (Figure 5e). The excluded charge obtained from 458 events generated a single distribution suggesting that no AuNP dimers were formed (Figure S12, Supporting Information). These data taken together signify single-particle detection via SERS in combination with electrical signal read-out from a nanopipet. The benefit of using both measurements is that AuNP shapes/sizes can be quantified through ionic current measurements and be used to normalize the SERS signal based on the characteristics of the plasmonic structure. The goal is to make SERS measurements more reproducible, which is a long-standing problem with low-concentration samples.[13,36] Furthermore, particles can be manipulated on-demand using DEP trapping to control AuNP aggregate formation and attraction toward the nanopipet tip.

CONCLUSION

In summary, we have demonstrated the use of nanopipets for two avenues of research. The first is the in situ on-demand formation of a SERS substrate by utilizing DEP acting on gold nanoparticles. An in-depth focus was placed on the magnitude of SERS enhancement, kinetics of substrate formation, and the effect of experimental factors, including the gap distance between electrodes. Second, TERS interactions were observed as individual nanoparticles translocated through the gold-coated nanopores, while ionic current measurements also provided a way to characterize the translocating nanostructures. This work marks a significant improvement over existing plasmonic nanopore structures through the addition of dielectrophoresis-based preconcentration of gold nanoparticles. Preconcentration of metallic features within a specific 3D space can be used in (1) SERS measurements and/or (2) ionic current/translocation measurements. In both cases, the time required to make a measurement is reduced since there are more molecules and/or events being positioned near the sensor. These attributes are important for any droplet or single-cell-based approaches, where a target molecule exists in solution and in low concentrations. We believe that these unique findings open the door to a broad range of applications, including multiplexed SERS detection, endoscopic measurements in single cells, and high-throughput/low-volume diagnostics.

METHODS

Fabrication. Nanopipets were fabricated using a Sutter P2000 pipet puller using quartz capillaries with an outer diameter of 1 mm and an inner diameter of 0.6 mm. The pulling conditions followed a two-line protocol: (1) HEAT: 575; FIL: 3; VEL: 35; DEL: 145; PUL: 75, followed by (2) HEAT: 600; FIL: 0; VEL: 15; DEL: 128; PUL: 200. Pipets were coated with 5 nm of gold (Quorum Technologies; Q150R S) and used immediately (although not required). In rare cases (approximately one in 20 pipets), gold would delaminate from the pipet, and this was observed optically by AuNPs being attracted upstream from the tip to where the gold layer was still intact. It was more likely to see the delamination of gold from the second gold electrode: a glass slide coated with 5−10 nm of gold.

AuNP Synthesis. Citrate-stabilized NPs were synthesized using the Turkevich−Frens method.[51,52] Briefly, 17.2 mg of $HAuCl_4$ (Sigma) was initially dispersed in 195 mL of DI H_2O. Afterward 11.2 mg of trisodium citrate dehydrate (Sigma) dissolved in 5 mL of H_2O was added. The solution was brought to reflux for 15 min followed by 2 h of cooling. The AuNPs were filtered using a 200 nm filter to remove any aggregated particles. Typical NP concentrations at the end of this protocol were between 70 and 90 pM using extinction spectroscopy. NP size after synthesis and filtering was measured to be 43 nm using SEM. A 20 μL amount of MGITC (1.2 μM) was added to 1 mL of NPs while mixing. This resulted in approximately ∼297 MGITC molecules/particle, if all dye molecules adsorbed onto each NP equally.

SERS Data Acquisition and Analysis. SERS measurements were performed on a home-built Raman microscope using a 632.8 nm wavelength excitation source, coupled to an inverted optical microscope.[53] The light was focused onto a 50 μm entrance slit of a spectrograph (303 mm focal length, Shamrock SR-303i, Andor) coupled to an electron multiplying

DOI: 10.1021/acsphotonics.6b00119
ACS Photonics 2016, 3, 1036−1044

charge coupled device (Newton DU970BV, Andor). Event rate was calculated by applying a threshold to photon count time traces and sorting independent events from background noise. The resulting number of events was divided by the time of the recording to find the event rate within each file.

Single-Channel Recordings. Ionic current was recorded using a patch clamp amplifier (Axopatch 200B) and digitized at a sampling frequency of 200 kHz and lowpass filter of 10 kHz (Digidata 1440). KCl solutions were prepared fresh prior to experiments and were placed within nanopipets after 10 min of plasma treatment. Event rate was calculated as described in the SERS analysis methods.

■ ASSOCIATED CONTENT

Supporting Information

The Supporting Information is available free of charge on the ACS Publications website at DOI: 10.1021/acsphotonics.6b00119.

Nanopipet/nanoparticle characterization, control Raman spectra, additional simulation results, particle diffusion modeling, agglomeration growth imaging, and additional translocation data (PDF)

■ AUTHOR INFORMATION

Corresponding Author

*E-mail: joshua.edel@imperial.ac.uk.

Author Contributions

⊥K. J. Freedman and C. R. Crick contributed equally.

Notes

The authors declare no competing financial interest.

■ ACKNOWLEDGMENTS

K.J.F. acknowledges support of the IIE's Whitaker International Program. J.B.E. acknowledges BBSRC and the receipt of an ERC starting investigator grant. S.H.O. acknowledges support from the U.S. National Science Foundation (NSF CAREER Award #DBI 1054191). S.A.M. acknowledges the EPSRC Reactive Plasmonics Program EP/M013812/1, the Leverhulme Trust, the Royal Society, and the Lee-Lucas Chair. A.B. acknowledges support from the University of Minnesota Doctoral Dissertation Fellowship. Part of the computational modeling was carried out using COMSOL software provided by the University of Minnesota Supercomputing Institute.

■ REFERENCES

(1) Fang, J.; Du, S.; Lebedkin, S.; Li, Z.; Kruk, R.; Kappes, M.; Hahn, H. Gold mesostructures with tailored surface topography and their self-assembly arrays for surface-enhanced Raman spectroscopy. *Nano Lett.* **2010**, *10*, 5006−5013.

(2) Smythe, E. J.; Dickey, M. D.; Bao, J.; Whitesides, G. M.; Capasso, F. Optical antenna arrays on a fiber facet for in situ surface-enhanced Raman scattering detection. *Nano Lett.* **2009**, *9*, 1132−1138.

(3) Lipomi, D. J.; Martinez, R. V.; Kats, M. A.; Kang, S. H.; Kim, P.; Aizenberg, J.; Capasso, F.; Whitesides, G. M. Patterning the tips of optical fibers with metallic nanostructures using nanoskiving. *Nano Lett.* **2010**, *11*, 632−636.

(4) Gottheim, S.; Zhang, H.; Govorov, A. O.; Halas, N. J. Fractal nanoparticle plasmonics: The Cayley tree. *ACS Nano* **2015**, *9*, 3284−3292.

(5) Stöckle, R. M.; Suh, Y. D.; Deckert, V.; Zenobi, R. Nanoscale chemical analysis by tip-enhanced Raman spectroscopy. *Chem. Phys. Lett.* **2000**, *318*, 131−136.

(6) Bouhelier, A.; Beversluis, M.; Hartschuh, A.; Novotny, L. Near-field second-harmonic generation induced by local field enhancement. *Phys. Rev. Lett.* **2003**, *90*, 013903.

(7) Lindquist, N. C.; Nagpal, P.; Lesuffleur, A.; Norris, D. J.; Oh, S.-H. Three-dimensional plasmonic nanofocusing. *Nano Lett.* **2010**, *10*, 1369−1373.

(8) Barik, A.; Cherukulappurath, S.; Wittenberg, N. J.; Johnson, T. W.; Oh, S.-H. Dielectrophoresis-assisted Raman spectroscopy of intravesicular analytes on metallic pyramids. *Anal. Chem.* **2016**, *88*, 1704−1710.

(9) Squires, T. M.; Messinger, R. J.; Manalis, S. R. Making it stick: convection, reaction and diffusion in surface-based biosensors. *Nat. Biotechnol.* **2008**, *26*, 417−426.

(10) Guarrotxena, N.; Bazan, G. C. Antitags: SERS-Encoded Nanoparticle Assemblies that Enable Single-Spot Multiplex Protein Detection. *Adv. Mater.* **2014**, *26*, 1941−1946.

(11) Liu, H.; Zhang, L.; Lang, X.; Yamaguchi, Y.; Iwasaki, H.; Inouye, Y.; Xue, Q.; Chen, M. Single molecule detection from a large-scale SERS-active $Au_{79}Ag_{21}$ substrate. *Sci. Rep.* **2011**, 110.1038/srep00112.

(12) Kneipp, K.; Wang, Y.; Kneipp, H.; Perelman, L. T.; Itzkan, I.; Dasari, R. R.; Feld, M. S. Single molecule detection using surface-enhanced Raman scattering (SERS). *Phys. Rev. Lett.* **1997**, *78*, 1667.

(13) Le Ru, E. C.; Grand, J.; Sow, I.; Somerville, W. R.; Etchegoin, P. G.; Treguer-Delapierre, M.; Charron, G.; Félidj, N.; Lévi, G.; Aubard, J. A scheme for detecting every single target molecule with surface-enhanced Raman spectroscopy. *Nano Lett.* **2011**, *11*, 5013−5019.

(14) Nie, S.; Emory, S. R. Probing single molecules and single nanoparticles by surface-enhanced Raman scattering. *Science* **1997**, *275*, 1102−1106.

(15) Zhang, Y.; Zhen, Y.-R.; Neumann, O.; Day, J. K.; Nordlander, P.; Halas, N. J. Coherent anti-Stokes Raman scattering with single-molecule sensitivity using a plasmonic Fano resonance. *Nat. Commun.* **2014**, 5.10.1038/ncomms5424

(16) Kneipp, J.; Kneipp, H.; Kneipp, K. SERS—a single-molecule and nanoscale tool for bioanalytics. *Chem. Soc. Rev.* **2008**, *37*, 1052−1060.

(17) Camden, J. P.; Dieringer, J. A.; Wang, Y.; Masiello, D. J.; Marks, L. D.; Schatz, G. C.; Van Duyne, R. P. Probing the structure of single-molecule surface-enhanced Raman scattering hot spots. *J. Am. Chem. Soc.* **2008**, *130*, 12616−12617.

(18) Cecchini, M. P.; Turek, V. A.; Paget, J.; Kornyshev, A. A.; Edel, J. B. Self-assembled nanoparticle arrays for multiphase trace analyte detection. *Nat. Mater.* **2013**, *12*, 165−171.

(19) Thacker, V. V.; Herrmann, L. O.; Sigle, D. O.; Zhang, T.; Liedl, T.; Baumberg, J. J.; Keyser, U. F. DNA origami based assembly of gold nanoparticle dimers for surface-enhanced Raman scattering. *Nat. Commun.* **2014**, 5.10.1038/ncomms4448

(20) Kühler, P.; Roller, E.-M.; Schreiber, R.; Liedl, T.; Lohmüller, T.; Feldmann, J. Plasmonic DNA-origami nanoantennas for surface-enhanced Raman spectroscopy. *Nano Lett.* **2014**, *14*, 2914−2919.

(21) Freedman, K. J.; Otto, L. M.; Ivanov, A. P.; Barik, A.; Oh, S.-H.; Edel, J. B. Nanopore sensing at ultra-low concentrations using single-molecule dielectrophoretic trapping. *Nat. Commun.* **2016**, *7*, 10217.

(22) Hermanson, K. D.; Lumsdon, S. O.; Williams, J. P.; Kaler, E. W.; Velev, O. D. Dielectrophoretic assembly of electrically functional microwires from nanoparticle suspensions. *Science* **2001**, *294*, 1082−1086.

(23) Chansin, G. A.; Mulero, R.; Hong, J.; Kim, M. J.; Demello, A. J.; Edel, J. B. Single-molecule spectroscopy using nanoporous membranes. *Nano Lett.* **2007**, *7*, 2901−2906.

(24) Pitchford, W. H.; Kim, H.-J.; Ivanov, A. P.; Kim, H.-M.; Yu, J.-S.; Leatherbarrow, R. J.; Albrecht, T.; Kim, K.-B.; Edel, J. B. Synchronized optical and electronic detection of biomolecules using a low noise nanopore platform. *ACS Nano* **2015**, *9*, 1740−1748.

(25) Nicoli, F.; Verschueren, D.; Klein, M.; Dekker, C.; Jonsson, M. P. DNA Translocations through Solid-State Plasmonic Nanopores. *Nano Lett.* **2014**, *14*, 6917−6925.

(26) Vitol, E. A.; Orynbayeva, Z.; Bouchard, M. J.; Azizkhan-Clifford, J.; Friedman, G.; Gogotsi, Y. In situ intracellular spectroscopy with

DOI: 10.1021/acsphotonics.6b00119
ACS Photonics 2016, 3, 1036−1044

surface enhanced Raman spectroscopy (SERS)-enabled nanopipettes. *ACS Nano* **2009**, *3*, 3529−3536.
(27) Masson, J.-F.; Breault-Turcot, J.; Faid, R.; Poirier-Richard, H.-P.; Yockell-Lelièvre, H.; Lussier, F. l.; Spatz, J. P. Plasmonic nanopipette biosensor. *Anal. Chem.* **2014**, *86*, 8998−9005.
(28) Ivanov, A. P.; Actis, P.; Jönsson, P.; Klenerman, D.; Korchev, Y.; Edel, J. B. On-demand delivery of single DNA molecules using nanopipets. *ACS Nano* **2015**, *9*, 3587−3595.
(29) Gong, X.; Patil, A. V.; Ivanov, A. P.; Kong, Q.; Gibb, T.; Dogan, F.; deMello, A. J.; Edel, J. B. Label-free in-flow detection of single DNA molecules using glass nanopipettes. *Anal. Chem.* **2013**, *86*, 835−841.
(30) Hernández-Ainsa, S.; Bell, N. A.; Thacker, V. V.; Göpfrich, K.; Misiunas, K.; Fuentes-Perez, M. E.; Moreno-Herrero, F.; Keyser, U. F. DNA origami nanopores for controlling DNA translocation. *ACS Nano* **2013**, *7*, 6024−6030.
(31) Hennig, S.; van de Linde, S.; Bergmann, S.; Huser, T.; Sauer, M. Quantitative Super-Resolution Microscopy of Nanopipette-Deposited Fluorescent Patterns. *ACS Nano* **2015**, *9*, 8122−8130.
(32) Steinbock, L. J.; Otto, O.; Chimerel, C.; Gornall, J.; Keyser, U. F. Detecting DNA folding with nanocapillaries. *Nano Lett.* **2010**, *10*, 2493−2497.
(33) Yang, Z.; Aizpurua, J.; Xu, H. Electromagnetic field enhancement in TERS configurations. *J. Raman Spectrosc.* **2009**, *40*, 1343−1348.
(34) Domke, K. F.; Zhang, D.; Pettinger, B. Toward Raman fingerprints of single dye molecules at atomically smooth Au (111). *J. Am. Chem. Soc.* **2006**, *128*, 14721−14727.
(35) Pieczonka, N. P.; Aroca, R. F. Single molecule analysis by surfaced-enhanced Raman scattering. *Chem. Soc. Rev.* **2008**, *37*, 946−954.
(36) Le Ru, E. C.; Etchegoin, P. G. Single-molecule surface-enhanced Raman spectroscopy. *Annu. Rev. Phys. Chem.* **2012**, *63*, 65−87.
(37) Huber, D. L.; Manginell, R. P.; Samara, M. A.; Kim, B.-I.; Bunker, B. C. Programmed adsorption and release of proteins in a microfluidic device. *Science* **2003**, *301*, 352−354.
(38) Cho, H.; Lee, B.; Liu, G. L.; Agarwal, A.; Lee, L. P. Label-free and highly sensitive biomolecular detection using SERS and electrokinetic preconcentration. *Lab Chip* **2009**, *9*, 3360−3363.
(39) Kumar, S.; Cherukulappurath, S.; Johnson, T. W.; Oh, S.-H. Millimeter-sized suspended plasmonic nanohole arrays for surface-tension-driven flow-through SERS. *Chem. Mater.* **2014**, *26*, 6523−6530.
(40) Cherukulappurath, S.; Lee, S. H.; Campos, A.; Haynes, C. L.; Oh, S.-H. Rapid and sensitive in situ SERS detection using dielectrophoresis. *Chem. Mater.* **2014**, *26*, 2445−2452.
(41) Jose, J.; Kress, S.; Barik, A.; Otto, L. M.; Shaver, J.; Johnson, T. W.; Lapin, Z. J.; Bharadwaj, P.; Novotny, L.; Oh, S.-H. Individual template-stripped conductive gold pyramids for tip-enhanced dielectrophoresis. *ACS Photonics* **2014**, *1*, 464−470.
(42) Pettinger, B.; Ren, B.; Picardi, G.; Schuster, R.; Ertl, G. Nanoscale probing of adsorbed species by tip-enhanced Raman spectroscopy. *Phys. Rev. Lett.* **2004**, *92*, 096101.
(43) Yeo, W.-H.; Kopacz, A. M.; Kim, J.-H.; Chen, X.; Wu, J.; Gao, D.; Lee, K.-H.; Liu, W.-K.; Chung, J.-H. Dielectrophoretic concentration of low-abundance nanoparticles using a nanostructured tip. *Nanotechnology* **2012**, *23*, 485707.
(44) Singhal, R.; Orynbayeva, Z.; Sundaram, R. V. K.; Niu, J. J.; Bhattacharyya, S.; Vitol, E. A.; Schrlau, M. G.; Papazoglou, E. S.; Friedman, G.; Gogotsi, Y. Multifunctional carbon-nanotube cellular endoscopes. *Nat. Nanotechnol.* **2011**, *6*, 57−64.
(45) Cecchini, M. P.; Wiener, A.; Turek, V. A.; Chon, H.; Lee, S.; Ivanov, A. P.; McComb, D. W.; Choo, J.; Albrecht, T.; Maier, S. A. Rapid ultrasensitive single particle surface-enhanced Raman spectroscopy using metallic nanopores. *Nano Lett.* **2013**, *13*, 4602−4609.
(46) Belaidi, S.; Girard, P.; Leveque, G. Electrostatic forces acting on the tip in atomic force microscopy: Modelization and comparison with analytic expressions. *J. Appl. Phys.* **1997**, *81*, 1023−1030.
(47) Barik, A.; Otto, L. M.; Yoo, D.; Jose, J.; Johnson, T. W.; Oh, S.-H. Dielectrophoresis-enhanced plasmonic sensing with gold nanohole arrays. *Nano Lett.* **2014**, *14*, 2006−2012.
(48) Honegger, T.; Berton, K.; Picard, E.; Peyrade, D. Determination of Clausius−Mossotti factors and surface capacitances for colloidal particles. *Appl. Phys. Lett.* **2011**, *98*, 181906.
(49) Wanunu, M.; Sutin, J.; McNally, B.; Chow, A.; Meller, A. DNA translocation governed by interactions with solid-state nanopores. *Biophys. J.* **2008**, *95*, 4716−4725.
(50) Belkin, M.; Chao, S.-H.; Jonsson, M. P.; Dekker, C.; Aksimentiev, A. Plasmonic nanopores for trapping, controlling displacement, and sequencing of DNA. *ACS Nano* **2015**, *9*, 10598−10611.
(51) Turkevich, J.; Stevenson, P. C.; Hillier, J. A study of the nucleation and growth processes in the synthesis of colloidal gold. *Discuss. Faraday Soc.* **1951**, *11*, 55−75.
(52) Frens, G. Controlled nucleation for the regulation of the particle size in monodisperse gold suspensions. *Nature, Phys. Sci.* **1973**, *241*, 20−22.
(53) Crick, C. R.; Albella, P.; Ng, B.; Ivanov, A. P.; Roschuk, T.; Cecchini, M. P.; Bresme, F.; Maier, S. A.; Edel, J. B. Precise attoliter temperature control of nanopore sensors using a nanoplasmonic bullseye. *Nano Lett.* **2014**, *15*, 553−559.

DOI: 10.1021/acsphotonics.6b00119
ACS Photonics 2016, 3, 1036−1044